Antenna Q and stored energy expressed in the fields, currents, and input impedance

Gustafsson, Mats; Jonsson, B.L.G

Published in:
IEEE Transactions on Antennas and Propagation

DOI:
10.1109/TAP.2014.2368111

2015

Document Version:
Peer reviewed version (aka post-print)

Antenna Q and stored energy expressed in the fields, currents, and input impedance

Mats Gustafsson, *Member, IEEE* and B. L. G. Jonsson

***Abstract*—Although the stored energy of an antenna is instrumental in the evaluation of antenna Q and the associated physical bounds, it is difficult to strictly define stored energy. Classically, the stored energy is either determined from the input impedance of the antenna or the electromagnetic fields around the antenna. The new energy expressions proposed by Vandenbosch express the stored energy in the current densities in the antenna structure. These expressions are equal to the stored energy defined from the difference between the energy density and the far field energy for many but not all cases. Here, the different approaches to determine the stored energy are compared for dipole, loop, inverted L-antennas, and bow-tie antennas. We use Brune synthesized circuit models to determine the stored energy from the input impedance. We also compare the results with differentiation of the input impedance and the obtained bandwidth. The results indicate that the stored energy in the fields, currents, and circuit models agree well for small antennas. For higher frequencies, the stored energy expressed in the currents agrees with the stored energy determined from Brune synthesized circuit models whereas the stored energy approximated by differentiation of input impedance gives a lower value for some cases. The corresponding results for the bandwidth suggest that the inverse proportionality between the fractional bandwidth and Q-factor depends on the threshold level of the reflection coefficient.**

***Index Terms*—Stored energy, Antenna Q, Antenna theory, Brune Synthesis**

I. Introduction

STORED electromagnetic energy is instrumental in determination of lower bounds on the Q-factor for antennas. The classical results by Chu [1] and Collin & Rothschild [2] are based on subtraction of the power flow and explicit calculations using mode expansions of the stored energy outside a sphere. This gives simple expressions for the minimum Q of small spherical antennas [1, 2]. The major shortcoming is that the results are restricted to spherical regions although some results for spheroidal regions are presented in [3, 4]. The results have also been generalized to the case with electric current sheets by Thal [5]. Yaghjian and Best [6] analyze stored energy for general media and its relation to the input impedance. The new expressions by Vandenbosch [7] are useful as they express the stored energy in the current density on the antenna structure. This has been shown to be instrumental in the analysis of small antennas [8–11] and also for antenna optimization [11–13]. The expressions have been verified for wire antennas in [14] and applied to characteristic modes in [10]. One minor problem with the proposed expressions is that they can produce negative values of stored energy for electrically large structures [9]. Alternative definitions and derivations of the stored energy are presented in [10, 15–20].

In this paper, we investigate the stored electric and magnetic energy expressions recently proposed by Vandenbosch [7]. We compare these expressions with the stored energy defined from subtraction of the energy density by the energy density in the far-field term [16]. The results provide a new interpretation of Vandenbosch's expressions [7] and explain the observed cases with negative stored energy [9]. We use Brune synthesis [21] to construct equivalent lumped circuit models from the input impedance, over a wide frequency band to accurately account for the stored energy of the antenna. The numerical results indicate that the stored energy in the circuit elements agree well with the stored energy in [7]. The results also show that the Q-factor calculated from differentiation of the input impedance, $Q_{\mathrm{Z}'}$, agrees with the Q-factor computed from the stored energy in the Brune circuit, $Q_{\mathrm{Z_B}}$, if Q is large and dominated by a single resonance. The values start to differ for lower values of Q where multiple resonances are common [22, 23].

We also compare the corresponding bandwidth with and without matching networks. The results indicate that the inverse proportionality between the fractional bandwidth $B \sim 1/Q$ is most accurate using $Q = Q_{\mathrm{Z}'}$ for relative narrow bandwidths $B < 2/Q$ whereas $Q = Q_{\mathrm{Z_B}}$ is better for wider bandwidths. This is consistent with $Q_{\mathrm{Z}'}$ being a local function of the input impedance and $Q_{\mathrm{Z_B}}$ depending on the global (all spectrum) behavior of the input impedance. The bandwidth for a simple shunt and series resonance circuit [22] is also analyzed using matching networks and Fano matching bounds [22, 24–26] to illustrate a case with $Q_{\mathrm{Z}'} \approx 0$, where the inverse proportionality of the fractional bandwidth to Q fails for $Q_{\mathrm{Z}'}$.

The paper is organized as follows. In Sec. II, the stored energy defined by subtraction of the far-field and stored energy expressed in the current density are analyzed. The coordinate dependence is also discussed. Stored energy from Brune synthesized circuits of the antenna input impedance is analyzed in Sec. III. Comparisons with numerical results for dipole, bow-tie, loop, and inverted L antennas are given in Sec. IV. The paper is concluded in Sec. V.

Manuscript received November 3, 2014. This work was supported by the Swedish Research Council (VR), the Swedish Foundation for Strategic Research, and Vinnova.

Mats Gustafsson is with the Department of Electrical and Information Technology, Lund University, Box 118, SE-221 00 Lund, Sweden. (Email: mats.gustafsson@eit.lth.se).

B. L. G. Jonsson is with the School of Electrical Engineering, KTH Royal Institute of Technology, Teknikringen 33, SE-100 44 Stockholm, Sweden. (Email: lars.jonsson@ee.kth.se)

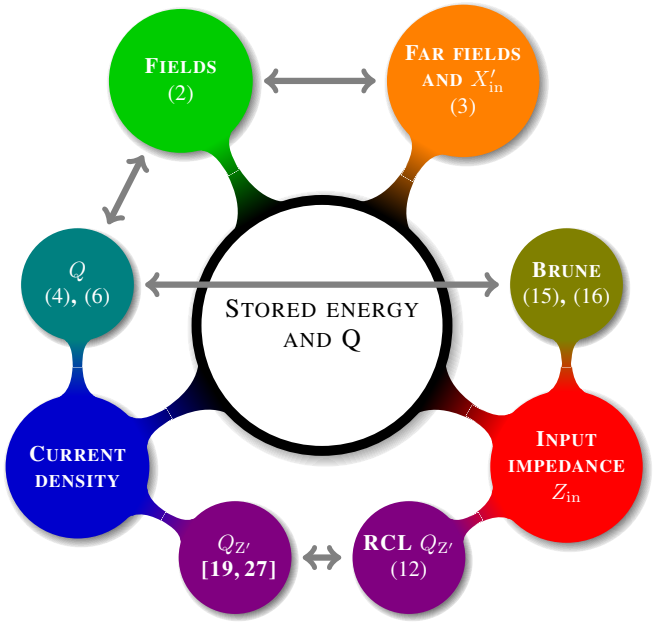

Fig. 1. Illustration of different approaches to estimate the stored energy and antenna Q. The classical approach in [6, 28] is based on subtraction of the far-field term (2) and expresses the stored energy in the frequency derivatives of the far-fields and reactance (3). Stored energy expressed in the current density (4) is *e.g.*, used in [7, 9–11, 16, 27, 29, 30]. Circuit models synthesized from the input impedance are considered in [1, 5, 22, 31] and Sec. III. Here, we discuss the relation between the Q-factors expressed in the currents, fields, reactance, and Brune circuits.

II. Stored Electromagnetic Energy

We consider time-harmonic electric, $\boldsymbol{E}(\boldsymbol{r})$, and magnetic, $\boldsymbol{H}(\boldsymbol{r})$, fields and current density $\boldsymbol{J}(\boldsymbol{r})$, with a suppressed $\mathrm{e}^{\mathrm{j}\omega t}$ dependence, where ω denotes the angular frequency and t time. For simplicity, we interchange between the angular frequency and the free space wavenumber $k = \omega/\mathrm{c}_0$, where the speed of light $\mathrm{c}_0 = 1/\sqrt{\mu_0\epsilon_0}$ and ϵ_0, μ_0, and $\eta_0 = \sqrt{\mu_0/\epsilon_0}$ are the free space permittivity, permeability, and impedance, respectively.

The electromagnetic energy in free space is the integral of the electric, $\epsilon_0|\boldsymbol{E}|^2/4$, and magnetic, $\mu_0|\boldsymbol{H}|^2/4$, energy densities. This electromagnetic energy increases to infinity as the region approaches $\mathbb{R}^3$ for time harmonic sources as the electric field approaches $\boldsymbol{E}(\boldsymbol{r}) \sim \mathrm{e}^{-\mathrm{j}kr}\boldsymbol{F}(\hat{\boldsymbol{r}})/r$ as $r \to \infty$, where $\boldsymbol{F}$ is the far-field, $r = |\boldsymbol{r}|$ and $\hat{\boldsymbol{r}} = \boldsymbol{r}/r$. The total electromagnetic energy is dominated by the energy in the radiated field far away from the antenna and is hence dissipated. The stored electromagnetic energy refers to the part of the electromagnetic energy that is not dissipated from the antenna. This quotient between the stored and dissipated power defines the Q-factor that can be written $Q = \max\{Q^{(\mathrm{E})}, Q^{(\mathrm{M})}\}$, where

$$Q^{(\mathrm{E})} = \frac{2\omega W^{(\mathrm{E})}}{P_{\mathrm{r}}}, \quad Q^{(\mathrm{M})} = \frac{2\omega W^{(\mathrm{M})}}{P_{\mathrm{r}}}, \tag{1}$$

and $W^{(\mathrm{E})}$ is the stored electric energy, $W^{(\mathrm{M})}$ the stored magnetic energy, and P_{r} the dissipated (radiated for a lossless antenna) power.

The stored energy can be estimated by circuit models from the input impedance [1, 5, 22, 31], the far field and reactance [6, 28], and the current density [7, 16, 17, 27, 32], see Fig. 1. As there are different approaches to estimate the stored energy, it is essential to investigate their pros and cons and their relation. Here, we compare the stored energy expressed in the fields, reactance and far field, and current densities. Moreover, we compare the Q-factor obtained from the current densities with the Q-factor obtained from Brune synthesized circuits numerically. The Q-factor computed from the differentiated input impedance [6] is also expressed in the current density in [19, 27], see Fig. 1.

Collin and Rothschild [2, 33] defined the stored energy by subtraction of the power flow. An alternative definition of the stored energy is used by Fante [28], Yaghjian and Best [6], where the far field energy density is subtracted

$$W_{\mathrm{F}}^{(\mathrm{E})} = \frac{\epsilon_0}{4}\int_{\mathbb{R}^3_{\mathrm{r}}} |\boldsymbol{E}(\boldsymbol{r})|^2 - \frac{|\boldsymbol{F}(\hat{\boldsymbol{r}})|^2}{r^2}\,\mathrm{dV} \tag{2}$$

and the integration is over the infinite sphere $\mathbb{R}^3_{\mathrm{r}}$. The subtracted far-field in the integrand can also be written as a subtraction of the radius times the radiated power [6]. The subtraction of the radiated energy flow is equivalent to subtraction of the energy density of the far field outside a circumscribing sphere. The stored magnetic energy, $W_{\mathrm{F}}^{(\mathrm{M})}$, is defined analogously.

A classical approach to analyze the stored energy is based on differentiation of the Maxwell equations. This leads to terms that include the feed current I_0, the frequency derivatives of the reactance, $X_{\mathrm{in}} = \operatorname{Im} Z_{\mathrm{in}}$, and the far field, $\boldsymbol{F}$ [6, 28]

$$W_{\mathrm{F}}^{(\mathrm{E})} = \frac{|I_0|^2}{4}X'_{\mathrm{in}} - \frac{1}{2\eta_0}\operatorname{Im}\int_{\Omega} \boldsymbol{F}'(\hat{\boldsymbol{r}})\cdot\boldsymbol{F}^*(\hat{\boldsymbol{r}})\,\mathrm{d}\Omega \tag{3}$$

for a self-resonant antenna, $W_{\mathrm{F}}^{(\mathrm{E})} = W_{\mathrm{F}}^{(\mathrm{M})}$, in free space, where $'$ denotes differentiation with respect to the angular frequency and * the complex conjugate. The energy expression is generalized to temporally dispersive bi-anisotropic material models in [6, 34] and shown to be coordinate dependent for some antennas [6].

The current based approach considered here is very different from (3) and expresses the stored energy as quadratic forms in the current density without using the input impedance and frequency derivatives. This makes the expressions directly applicable to current optimization [9, 11], where the optimal current distribution on the antenna structure is determined. The expressions are also useful in antenna optimization as the antenna Q is directly determined from a single frequency simulation [12, 13]. One common drawback with the two approaches comes from the basic definition of the stored energy as the energy density subtracted by the far-field energy. This term can be negative [9] and coordinate dependent [6, 16] as further discussed below.

The stored energy defined by subtraction of the far-field energy (2) can be written as the sum of a coordinate independent term $W_{\mathrm{C}}^{(\mathrm{E})}$ and a coordinate dependent term $W_{\mathrm{c},\mathbf{0}}$ [16], *i.e.*, $W_{\mathrm{F}}^{(\mathrm{E})} = W_{\mathrm{C}}^{(\mathrm{E})} + W_{\mathrm{c},\mathbf{0}}$. In [16], it is shown that the coordinate independent term $W_{\mathrm{C}}^{(\mathrm{E})}$ is identical to the stored

energy expressions introduced by Vandenbosch [7] and given by

$$W_{\mathrm{C}}^{(\mathrm{E})} = \frac{\eta_0}{4\omega} \int_V \int_V \nabla_1 \cdot \boldsymbol{J}_1 \nabla_2 \cdot \boldsymbol{J}_2^* \frac{\cos(kr_{12})}{4\pi k r_{12}} - \left(k^2 \boldsymbol{J}_1 \cdot \boldsymbol{J}_2^* - \nabla_1 \cdot \boldsymbol{J}_1 \nabla_2 \cdot \boldsymbol{J}_2^*\right) \frac{\sin(kr_{12})}{8\pi} \,\mathrm{dV}_1 \,\mathrm{dV}_2, \quad (4)$$

where $\boldsymbol{J}_n = \boldsymbol{J}(\boldsymbol{r}_n)$, $n = 1, 2$ and $r_{12} = |\boldsymbol{r}_1 - \boldsymbol{r}_2|$. This gives a direct interpretation of the integral expressions in [7, 16] as the coordinate independent part of (2) and of the negative stored energy in [9] from the subtraction of the far-field energy in the interior of the smallest circumscribing sphere [16]. The coordinate dependent part is [16]

$$W_{\mathrm{c},\mathbf{0}} = \frac{\eta_0}{4\omega} \int_V \int_V \mathrm{Im}\left\{k^2 \boldsymbol{J}(\boldsymbol{r}_1) \cdot \boldsymbol{J}^*(\boldsymbol{r}_2) - \nabla_1 \cdot \boldsymbol{J}(\boldsymbol{r}_1) \nabla_2 \cdot \boldsymbol{J}^*(\boldsymbol{r}_2)\right\} \frac{r_1^2 - r_2^2}{8\pi r_{12}} k \,\mathrm{j}_1(kr_{12}) \,\mathrm{dV}_1 \,\mathrm{dV}_2, \quad (5)$$

where $\mathrm{j}_1(z) = (\sin(z) - z\cos(z))/z^2$ is a spherical Bessel function.

The stored magnetic energy is similarly given by $W_{\mathrm{F}}^{(\mathrm{M})} = W_{\mathrm{C}}^{(\mathrm{M})} + W_{\mathrm{c},\mathbf{0}}$, where the coordinate independent part is

$$W_{\mathrm{C}}^{(\mathrm{M})} = \frac{\eta_0}{4\omega} \int_V \int_V k^2 \boldsymbol{J}_1 \cdot \boldsymbol{J}_2^* \frac{\cos(kr_{12})}{4\pi k r_{12}} - \left(k^2 \boldsymbol{J}_1 \cdot \boldsymbol{J}_2^* - \nabla_1 \cdot \boldsymbol{J}_1 \nabla_2 \cdot \boldsymbol{J}_2^*\right) \frac{\sin(kr_{12})}{8\pi} \,\mathrm{dV}_1 \,\mathrm{dV}_2 \,. \quad (6)$$

We also have the radiated power [7, 35]

$$P_{\mathrm{r}} = \frac{\eta_0}{2} \int_V \int_V \left(k^2 \boldsymbol{J}(\boldsymbol{r}_1) \cdot \boldsymbol{J}^*(\boldsymbol{r}_2) - \nabla_1 \cdot \boldsymbol{J}(\boldsymbol{r}_1) \nabla_2 \cdot \boldsymbol{J}^*(\boldsymbol{r}_2)\right) \frac{\sin(kr_{12})}{4\pi k r_{12}} \,\mathrm{dV}_1 \,\mathrm{dV}_2 \quad (7)$$

expressed as a quadratic form in $\boldsymbol{J}$.

One major difference between the expressions for $W_{\mathrm{F}}^{(\mathrm{E})}$ in (2), (3), and $W_{\mathrm{F}}^{(\mathrm{E})} = W_{\mathrm{C}}^{(\mathrm{E})} + W_{\mathrm{c},\mathbf{0}}$ is the coordinate dependence, see also Fig. 1. The stored electric and magnetic energies defined by subtraction of the far field (2) contain the potentially coordinate dependent part $W_{\mathrm{c},\mathbf{0}}$ defined in (5). Assume the term $W_{\mathrm{c},\mathbf{0}}$ for one coordinate system. Consider a shift of the coordinate system $\boldsymbol{r} \to \boldsymbol{d} + \boldsymbol{r}$ and use that $r_1^2 - r_2^2 \to r_1^2 - r_2^2 + 2\boldsymbol{d} \cdot (\boldsymbol{r}_1 - \boldsymbol{r}_2)$. This gives the coordinate dependent term [16]

$$W_{\mathrm{c},\boldsymbol{d}} = W_{\mathrm{c},\mathbf{0}} - k\boldsymbol{d} \cdot \frac{\epsilon_0}{4k} \int_\Omega \hat{\boldsymbol{r}} |\boldsymbol{F}(\hat{\boldsymbol{r}})|^2 \,\mathrm{d}\Omega. \quad (8)$$

The corresponding Q-factor is shifted as

$$\Delta Q_{\mathrm{c},\boldsymbol{d}} = \frac{-k\boldsymbol{d} \cdot \int_\Omega \hat{\boldsymbol{r}} |\boldsymbol{F}(\hat{\boldsymbol{r}})|^2 \,\mathrm{d}\Omega}{2\int_\Omega |\boldsymbol{F}(\hat{\boldsymbol{r}})|^2 \,\mathrm{d}\Omega}, \quad (9)$$

where we see that $|\Delta Q_{\mathrm{c},\boldsymbol{d}}| \leq ka$ for all coordinate shifts within the a circumscribing sphere with radius a. We note that this term is similar to the coordinate dependence observed in [6] from the far-field term in (3). The fundamental difference between the coordinate dependence of (3) and the current expression (5) is that the current based expressions has a natural decomposition in one coordinate independent term (4) and one coordinate dependent term (5) whereas (3) combines the two [6].

III. Stored energy from the input impedance

The bandwidth of an antenna is often determined from the antenna input impedance. The fractional bandwidth is related to the Q-value for single resonance circuits as [6]

$$B = \frac{\omega_2 - \omega_1}{\omega_0} \approx \frac{2\Gamma_0}{Q\sqrt{1 - \Gamma_0^2}}, \quad (10)$$

where $\omega_0 = (\omega_1 + \omega_2)/2$ and Γ_0 is the threshold of the reflection coefficient. Similarly, the Fano limit [22, 24–26] for a single resonance circuit, $B \leq 27.29/(Q|\Gamma_{0,\,\mathrm{dB}}|)$, is an upper bound on the bandwidth after matching, where $\Gamma_{0,\,\mathrm{dB}} = 20\log_{10}\Gamma_0$. For more general circuit networks, we consider the Q-values determined from the differentiated input impedance and the stored energy in equivalent circuit models, see also Fig. 1. The Q-factors calculated from the stored and dissipated energy are given by

$$Q^{(\mathrm{E})} = \frac{\sum_n |I_n|^2/C_n}{\omega \sum_n R_n |I_n|^2} \quad \text{and} \quad Q^{(\mathrm{M})} = \frac{\omega \sum_n L_n |I_n|^2}{\sum_n R_n |I_n|^2}, \quad (11)$$

where C_n, L_n, R_n, and I_n are the capacitance, inductance, resistance and current in branch n of the network. The Q factors determined from the differentiated input impedance is [6, 22]

$$Q_{\mathrm{Z}'} = \omega|\Gamma'| = \frac{\omega|Z_{\mathrm{t}}'|}{2R} = \frac{\sqrt{(\omega R')^2 + (\omega X' + |X|)^2}}{2R}, \quad (12)$$

where $'$ denotes differentiation with respect to ω, Z_{t} is the input impedance $Z_{\mathrm{in}} = R_{\mathrm{in}} + \mathrm{j}X_{\mathrm{in}}$ tuned to resonance with a lumped series (or analogous for lumped elements in parallel [19]) inductor or capacitor, and Γ the corresponding reflection coefficient. In addition to the Q-factor in (12), we determine the stored energy in the lumped element normalized with the radiated power as $|X_{\mathrm{in}}|/R_{\mathrm{in}}$ giving the electric and magnetic Q factors, *cf.*, (1)

$$Q_{\mathrm{Z}'}^{(\mathrm{E})} = \begin{cases} Q_{\mathrm{Z}'} & \text{if } X_{\mathrm{in}}(\omega_0) < 0 \\ Q_{\mathrm{Z}'} - |X_{\mathrm{in}}|/R_{\mathrm{in}} & \text{if } X_{\mathrm{in}}(\omega_0) > 0 \end{cases} \quad (13)$$

and

$$Q_{\mathrm{Z}'}^{(\mathrm{M})} = \begin{cases} Q_{\mathrm{Z}'} & \text{if } X_{\mathrm{in}}(\omega_0) > 0 \\ Q_{\mathrm{Z}'} - |X_{\mathrm{in}}|/R_{\mathrm{in}} & \text{if } X_{\mathrm{in}}(\omega_0) < 0, \end{cases} \quad (14)$$

respectively.

The $Q_{\mathrm{Z}'}$ expression can be interpreted as a local approximation of the input impedance with a Padé approximation and subsequent evaluation of the stored energy in the resulting RCL circuit [22]. An alternative way to estimate the Q-factor of an antenna is to synthesize a broadband circuit model of the input impedance and to determine the stored energy in the inductors and capacitors (11). The circuit models and their stored energy are in general non-unique. One can *e.g.*, easily construct a frequency independent purely resistive input

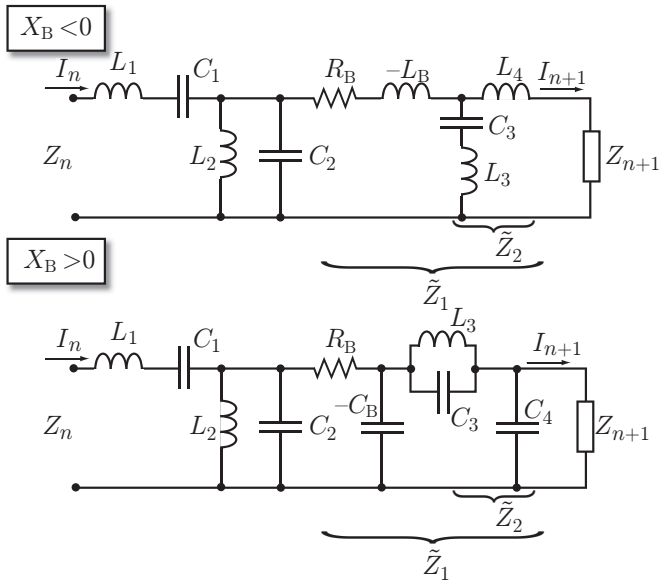

Fig. 2. Illustration of the Brune synthesis of a lumped circuit from a rational positive real (PR) input impedance $Z_\mathrm{in} = Z_1$. In each iteration step, $Z_n \to Z_{n+1}$, series and shunt capacitance and inductance are first removed. Then the series resistance $R_\mathrm{B} = \min_\omega \mathrm{Re}\, Z$ is removed. This leaves a PR function with $Z(\omega_0) = \mathrm{j}X_\mathrm{B}$. Depending on the sign of $X_\mathrm{B} = \mathrm{Im}\, Z(\omega_0)$ a negative inductance or capacitance is removed. Finally, a resonance LC circuit and series inductance or shunt capacitance are removed, see [21, 36] for details. Note, that the cases $R_\mathrm{B} = 0$ and $X_\mathrm{B} = 0$ are treated separately.

impedance lumped circuit network containing inductors and capacitors. Here, we consider Brune synthesis [21, 36] as an automated synthesis technique that does not produce such types of non-observable circuit networks.

The Brune circuit synthesis is based on expressing the input impedance as a (rational) positive real (PR) function in the complex frequency variable $s = \sigma + \mathrm{j}\omega$ and subsequent manipulation of the PR function to identify the circuit elements. This requires modeling over wide bandwidths and shows that the resulting Q-factor depends on the global (all spectrum) properties of the input impedance. We start to construct a rational approximation of the antenna input impedance. It is essential to have an accurate approximation from DC up to the frequencies of interest. In the range $0 \le \omega \le \omega_\mathrm{u}$ we use a rational function of order (m, n), with $|m - n| \le 1$, that is fitted to the input impedance using vector fitting [37, 38]. The order is chosen as low as possible such that the relative error is below some threshold, here we use 10^{-3}, and that the rational function is a PR function [21, 38].

Brune synthesis [21, 36] is an iterative procedure, where the order of the rational PR function modeling the input impedance is reduced in each step $Z_n \to Z_{n+1}$, see Fig. 2. Here, we only present a brief overview of the Brune synthesis for the purpose of calculating the stored energy, see [21, 36] for details. First, series (C_1, L_1) and shunt (C_2, L_2) capacitance and inductance are removed by identification of the asymptotic expansion of the input impedance and admittance at $s = 0$ and $s = \infty$. Then, the series resistance $R_\mathrm{B} = \min_{s=\mathrm{j}\omega} \mathrm{Re}\, Z$ is removed. This leaves a PR function with $Z(\mathrm{j}\omega_0) = \mathrm{j}X_\mathrm{B}$ at $\omega = \omega_0$. Depending on the sign of $X_\mathrm{B} = \mathrm{Im}\, Z(\mathrm{j}\omega_0)$ either a negative inductance or a negative capacitance is removed, see Fig. 2. Finally, a resonance LC circuit and series inductance or shunt capacitance are removed, see [21, 36] for details. Note, that also the cases $R_\mathrm{B} = 0$ and $X_\mathrm{B} = 0$ are treated separately. This leaves a PR function, Z_{n+1} of lower order than Z_n. The iteration, $Z_n \to Z_{n+1}$, is terminated when a purely resistive load remains, *i.e.*, $\mathrm{Im}\, Z_{n+1} = 0$.

The stored energy is easily calculated in the iterative synthesis procedure. The stored electric and magnetic energy in a capacitor, C, and inductor, L, are $W^{(\mathrm{E})} = |V|^2 C/4$ and $W^{(\mathrm{M})} = |I|^2 L/4$, respectively, where I denotes the current and V the voltage. For simplicity, consider the case with a series inductor, *i.e.*, $Z_\mathrm{B} = \mathrm{j}\omega L_\mathrm{B}$. The stored electric and magnetic energies are then iteratively given by

$$W^{(\mathrm{E})}_{\mathrm{B},n} = \frac{|I_n|^2}{4\omega^2 C_1} + \frac{|\widetilde{V}_1|^2 C_2}{4} + \frac{|\widetilde{V}_2|^2}{4\omega^2 C_3(\omega L_3 - \frac{1}{\omega C_3})^2} + W^{(\mathrm{E})}_{\mathrm{B},n+1} \quad (15)$$

and

$$W^{(\mathrm{M})}_{\mathrm{B},n} = \frac{L_1|I_n|^2}{4} + \frac{|\widetilde{V}_1|^2}{4\omega^2 L_2} + \frac{|\widetilde{V}_1|^2 L_\mathrm{B}}{4|\widetilde{Z}_1|^2} + \frac{|\widetilde{V}_2|^2 L_3}{4(\omega L_3 - \frac{1}{\omega C_3})^2} + \frac{|I_{n+1}|^2 L_4}{4} + W^{(\mathrm{M})}_{\mathrm{B},n+1}, \quad (16)$$

where $\widetilde{V}_n$ is the voltage over $\widetilde{Z}_n$ for $n = 1, 2$. One problem with the Brune synthesis is that it uses negative inductors L_B and capacitors C_B [21, 36], see also Fig. 2. This is resolved by transforming the *Tee* network containing the negative element to an ideal transformer, see App. A.

IV. Numerical examples

We consider a resonance circuit and dipole, bow-tie, loop, and inverted L antennas to illustrate the Q-factors determined from differentiation of the input impedance, the stored energies expressed in the current densities, and Brune synthesized circuits. For the antenna cases in Figs 4 to 8, we use solid curved for Q-factors from the current densities (4) and (6), dotted curved for the Brune circuits (11), and dash-dotted curves for the differentiated input impedance (13) and (14). Moreover, curves for the electric $Q^{(\mathrm{E})}$ and magnetic $Q^{(\mathrm{M})}$ factors (1) are labeled by (E) and (M), respectively.

A. Resonance circuit

The first example is a simple resonance circuit composed of cascaded shunt LC and series LC networks, see Fig. 3. This example extends the results in [22] and clearly illustrates the difference between $Q_{\mathrm{Z}'}$ and $Q_{\mathrm{Z_B}}$. In particular, the case $Q_{\mathrm{Z}'} = 0$ and resulting bandwidths after Fano matching are considered. The elements are chosen to have the same resonance frequency and the element values are expressed in the series Q_s and parallel Q_p Q-factors. The Q-factor determined from the stored energy, $Q_{\mathrm{Z_B}}$, in the circuit elements and from differentiation of the input impedance, $Q_{\mathrm{Z}'}$, are [22]

$$Q_{\mathrm{Z_B}} = Q_\mathrm{s} + Q_\mathrm{p} \quad \text{and} \quad Q_{\mathrm{Z}'} = |Q_\mathrm{s} - Q_\mathrm{p}|, \quad (17)$$

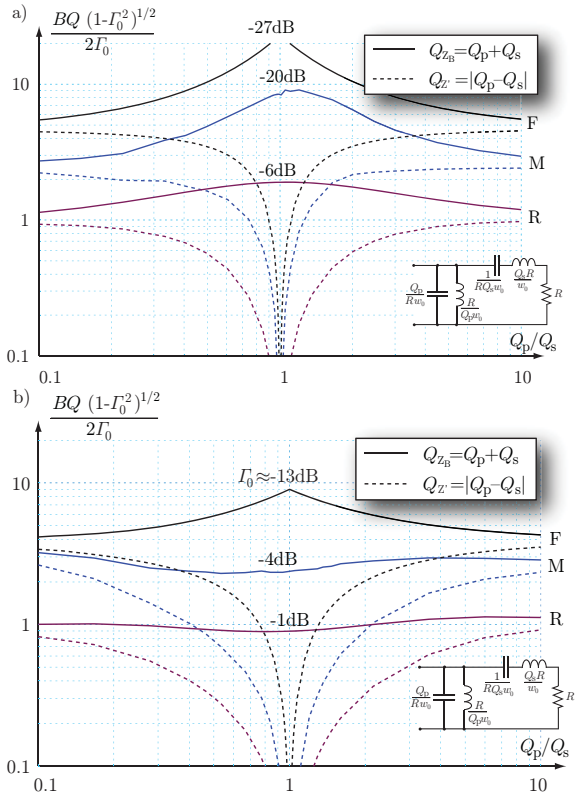

Fig. 3. Illustration of the Q-factor fractional bandwidth product for a cascaded shunt LC and series LC network, where the bandwidth is determined for the resonance model (R), matching network (M), and Bode-Fano limit (F). The Q factors are determined from the stored energies in the circuit elements and from differentiation of the input impedance (12). The maximal reflection coefficient is determined over the fractional bandwidths $B = \{2, 4\}/Q_{\mathrm{Z_B}}$ with and without matching networks for the case $Q_\mathrm{s} = 10$ and $1 \le Q_\mathrm{p} \le 100$. The matching network is determined using genetic algorithms with four ideal lumped elements. a) $B = 2/Q_{\mathrm{Z_B}}$ and b) $B = 4/Q_{\mathrm{Z_B}}$.

respectively. Here, we note that $Q_{\mathrm{Z_B}} \ge Q_{\mathrm{Z}'}$ and that $Q_{\mathrm{Z}'} = 0$ for the case of a flat match $Q_\mathrm{s} = Q_\mathrm{p}$.

The resulting bandwidth depends on the threshold of the reflection coefficient as seen for the simple RCL resonance circuit in (10). We illustrate the relation between Q and the fractional bandwidth B, by plotting $BQ\sqrt{1-\Gamma_0^2}/(2\Gamma_0)$ for $Q = \{Q_{\mathrm{Z_B}}, Q_{\mathrm{Z}'}\}$, *i.e.*, Q given by the stored energy in the circuit elements and by differentiation of the input impedance in (17), see Fig. 3. We consider the well matched case ($|\Gamma| \le -10\,\mathrm{dB}$) but narrow bandwidth and less well matched case ($|\Gamma| \le -3\,\mathrm{dB}$) and wider bandwidth to illustrate the dependence on $Q_{\mathrm{Z_B}}$ and $Q_{\mathrm{Z}'}$. The series Q value is fixed to $Q_\mathrm{s} = 10$ whereas the parallel Q-factor is in the range $1 \le Q_\mathrm{p} \le 100$. The curves labeled (R) show the unmatched bandwidth Q-factor product (10) for the fractional bandwidths $B = 2/Q_{\mathrm{Z_B}}$ and $B = 4/Q_{\mathrm{Z_B}}$.

We observe that the product is close to unity at the end points $Q_\mathrm{p} = \{1, 100\}$, where the input impedance resembles series and parallel RCL circuits, respectively. In the region $Q_\mathrm{p} \approx Q_\mathrm{s}$ the curves deviate from unity as the input impedance does not resemble an RCL resonance circuit. We also note that the approximation with $Q_{\mathrm{Z}'} = |Q_\mathrm{s} - Q_\mathrm{p}|$ gives vanishing small values showing that the $Q_{\mathrm{Z}'}$ approximation fails for this case [22]. The use of the Q-factor from the stored energy, $Q = Q_{\mathrm{Z_B}}$, gives better results. In particular for the wider bandwidth case $B = 4/Q_{\mathrm{Z_B}}$.

We also consider the case with matching circuits. The Bode-Fano matching limits [22, 24] are depicted by the curves labeled (F) for the cases $B = 2/Q_{\mathrm{Z_B}}$ and $B = 4/Q_{\mathrm{Z_B}}$. We use optimization to synthesize lossless matching networks. The curves labeled (M) in Fig. 3 show the resulting bandwidth Q-factor product (10) after matching. The first case gives a matching threshold Γ_0 in the range $-15\,\mathrm{dB}$ to $-20\,\mathrm{dB}$ whereas the second case gives Γ_0 in the range $-3\,\mathrm{dB}$ to $-6\,\mathrm{dB}$. We note that the Bode-Fano limit mainly depends on the maximal Q value that can be interpreted as the mean $\langle Q \rangle = (Q_{\mathrm{Z_B}} + Q_{\mathrm{Z}'})/2 = \max\{Q_\mathrm{p}, Q_\mathrm{s}\}$. A genetic algorithm [39] is used to determine the parameters of a matching network composed of up to two capacitors and two inductors.

The results show that the inverse proportionality between B and Q in (10) is valid for the resonance circuit case far away from $Q_\mathrm{s} = Q_\mathrm{p}$. Closer to $Q_\mathrm{s} = Q_\mathrm{p}$, the results are better for the stored energy, $Q_{\mathrm{Z_B}} = Q_\mathrm{s} + Q_\mathrm{p}$, than for the differentiated input impedance $Q_{\mathrm{Z}'} = |Q_\mathrm{s} - Q_\mathrm{p}|$. The addition of a matching network increases the bandwidth. Also for this case, the stored energy results are better although they underestimate the bandwidth with up to approximately a factor of two. It should also be noted that the addition of the matching network increases the stored energy and hence the $Q_{\mathrm{Z_B}}$, so the $Q_{\mathrm{Z_B}}$ after matching can underestimate the bandwidth even more.

B. Strip dipole antenna

Consider a center fed strip dipole with length ℓ and width $\ell/100$ modeled as a perfect electric conductor (PEC). The Q-factors (1) determined from the current expressions $Q_\mathrm{C}^{(\mathrm{E})}$ in (4) and $Q_\mathrm{C}^{(\mathrm{M})}$ in (6), the Brune synthesized circuit model (15) and (16), and differentiation of the input impedance (13) and (14) are all compared in Fig. 4. The Q-factors derived from the circuit model approximates the current expression well up to at least $\ell/\lambda = 3$. The Q-factor computed from the frequency differentiated input impedance is very close to the stored energy up to the resonance at half a wavelength and slightly lower for higher frequencies.

We also consider an off center fed strip dipole with length ℓ and width $\ell/100$. The feed is placed at the distance 0.27ℓ from the center and modeled as an ideal voltage gap. The stored energy is evaluated with the current expressions (4) and (6), a Brune synthesized circuit (15) and (16), and differentiation of the input impedance (13) and (14) for the wavelength (frequency) range $\ell \le 6\lambda$. The strip dipole is discretized into 100 rectangles and 200 rectangles with negligible differences in the results.

The resulting Q-values are depicted in Fig. 5. We observe that the Q-values from the current expressions and the Brune circuit agree well for the considered frequency range. Here, we note that it is essential to use an accurate approximating rational PR function from static up to the highest considered frequency. For the data in Fig. 5, we use a rational PR function of the order 20. The corresponding values from the

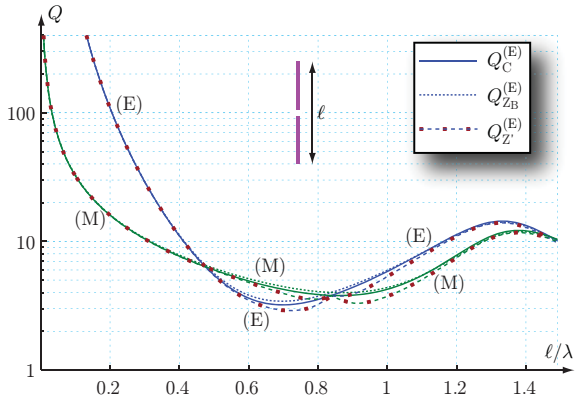

Fig. 4. Illustration of the Q-factor for a center fed strip dipole with length ℓ and width $\ell/100$. The Q factors are determined from the stored energies (4) and (6), the stored energy in the Brune synthesized lumped circuit model (15) and (16), and from differentiation of the input impedance (13) and (14).

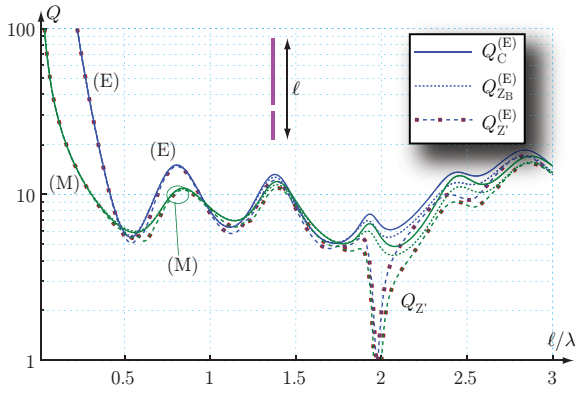

Fig. 5. Illustration of the Q-factor for a strip dipole with length ℓ and width $\ell/100$ fed 0.27ℓ from the center of the strip. The Q factors are determined from the current expressions (4) and (6), the Brune synthesized lumped circuit model (15) and (16), and from differentiation of the input impedance (13) and (14).

differentiated input impedance agree well for $\ell \leq 0.5\lambda$ and starts to deviate for higher frequencies. There is however a large deviation around $\ell \approx 2\lambda$, where $Q_{\mathrm{Z}'} \approx 0$. This resembles the lumped circuit case in Sec. IV-A, see also [22, 23].

C. Bow-tie antenna

The bow-tie antenna is a wide-band version of the dipole antenna. The computed Q-factors for a smooth bow-tie antenna is depicted in Fig. 6. The Q factors determined from the current expressions, the Brune synthesized lumped circuit model, and from differentiation of the input impedance agree for $\ell/\lambda < 0.4\ell$, where $Q > 5$. The Q-factor drops to below 2 for $\ell/\lambda > 0.5$, where the different Q-values start to deviate. Here, the use of Q to evaluate the performance of antennas is questionable and the inverse proportionality to the fractional bandwidth (10) is in general not valid. However, it is interesting to compare the Q-values given by the different approaches. In Fig. 6, we note that the Q-factors from the current expressions (4) and (6) gives the highest values with a $Q \approx 2$. The stored energy in the Brune synthesized circuits gives $Q \approx 1$, whereas the differentiated input impedance oscillates between 0.1 and 1.

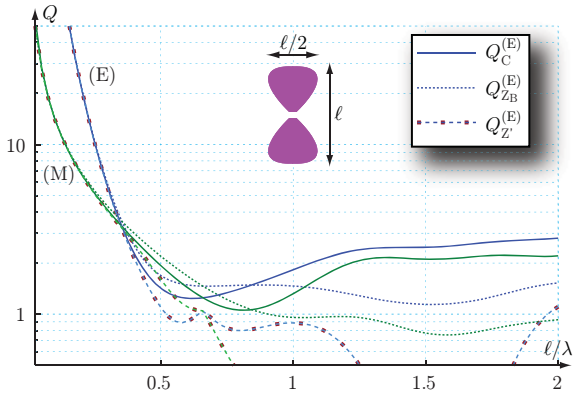

Fig. 6. Illustration of the Q-factor for a bow-tie antenna with length ℓ and width $\ell/2$. The Q factors are determined from the current expressions (4) and (6), the Brune synthesized lumped circuit model (15) and (16), and from differentiation of the input impedance (13) and (14).

We note that the absolute difference between Q_{C} and $Q_{\mathrm{Z_B}}$ is of the order one. This is similar to the observed difference in Fig. 5. The relative difference is however larger as the Q-factors are much lower. Although, the Q-values are very low, the example shows that the Q factors from the current densities and Brune circuits can differ. We have also considered higher orders of the Brune circuit and larger frequency intervals with similar results.

D. Loop antenna

The computed stored electric and magnetic energies for a loop antenna are depicted in Fig. 7. The strip loop antenna is rectangular with height ℓ, width $\ell/2$, strip width $\ell/64$, vanishing thickness, and is modeled as a perfect electric conductor (PEC). We see that the magnetic energy dominates for low frequencies. This changes to dominant electric energy at approximately $\lambda \approx 6\ell$ or equivalently $\mathcal{C} \approx \lambda/2$, where $\mathcal{C} = 3\ell$ denotes the circumference of the loop. The Q-factors determined from the stored energies (4) and (6) and from the Brune synthesized lumped circuit (15) and (16) agree very well. The Q factors also agree with the differentiation of the input impedance for $Q \geq 10$. The difference increases for lower Q values. This is consistent with the increasing difficulty to approximate the input impedance with a single resonance model [22]. Here, it is also important to realize that the concept and usefulness of the Q-factor is increasingly questionable as Q decreases towards unity.

E. Inverted L-antenna

An inverted L-antenna on a finite ground plane is considered to illustrate the usefulness of the stored energies for terminal antennas, see also [12, 13]. The structure has total length ℓ and width $\ell/2$. The inverted L fills the top 8% of the structure and consists of strips with widths $\ell/64$ and $\ell/32$, see Fig. 8. The electric and magnetic Q-factors are depicted as a function of ℓ/λ in Fig. 8. We see that Q_{C}, $Q_{\mathrm{Z_B}}$, and $Q_{\mathrm{Z}'}$ agree well for $Q \geq 10$, that is for approximately $\ell \leq \lambda/3$ or below $1\,\mathrm{GHz}$ for $10\,\mathrm{cm}$ chassis. The results for $Q_{\mathrm{Z}'}$ start to differ for larger

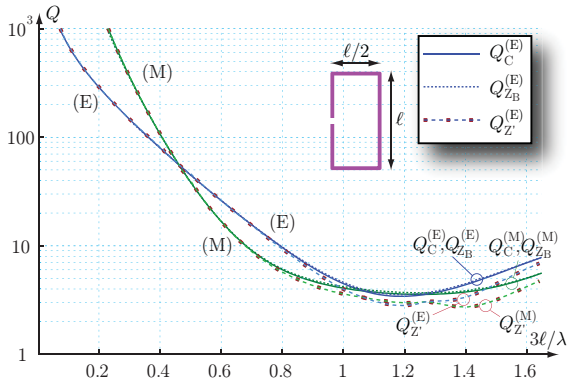

Fig. 7. Q factors for a rectangular loop antenna with height ℓ and width $\ell/2$. The Q factors are determined from the current expressions (4) and (6), the Brune synthesized lumped circuit model (15) and (16), and from differentiation of the input impedance (13) and (14).

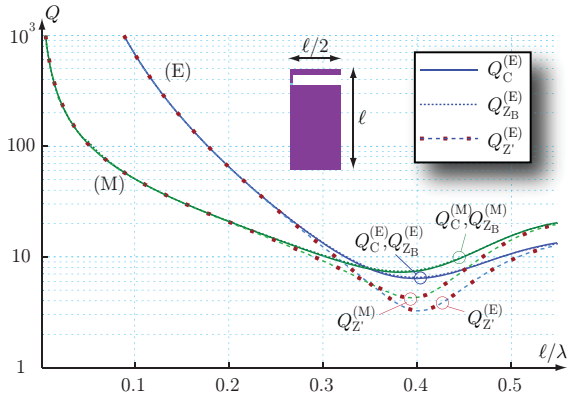

Fig. 8. Q factors for an inverted L antenna with height ℓ and width $\ell/2$. The Q factors are determined from the current expressions (4) and (6), the Brune synthesized lumped circuit model (15) and (16), and from differentiation of the input impedance (13) and (14).

structures, where *e.g.*, $Q_{\rm C}^{\rm (E)} \approx 5$ and $Q_{\rm Z'}^{\rm (E)} \approx 2$ at $\ell/\lambda = 0.4$ or $ka \approx 1.4$. For these levels of $Q_{\rm Z'}$, the underlying single resonance model [22] is problematic and hence $Q_{\rm Z'}$ reduces in accuracy. At the same time Q is low enough to be considered less useful as a quantity to estimate the bandwidth, *e.g.*, $Q \approx 2$ corresponds to a half-power bandwidth of 100%.

We use the fractional bandwidth for the antenna tuned to resonance with an inductor or capacitor to analyze the difference between the Q factors from the stored energy and differentiated input impedance. The fractional bandwidth Q-factor product, BQ, is given by (10) for simple RCL resonance circuits. The corresponding BQ product for the inverted L antenna is depicted in Fig. 9 for the reflection coefficient thresholds $\Gamma_0 = -\{1, 3, 10, 20\}$ dB. It is seen that BQ is close to the value given by (10) as indicated by the rhombi for $\ell/\lambda \leq 0.25$, where also $Q_{\rm C} \approx Q_{\rm Z_B} \approx Q_{\rm Z'}$. The BQ product starts to deviate from (10) for shorter wavelengths except for the low reflection coefficient $\Gamma_0 = -20$ dB and $Q_{\rm Z'}$ case. This is consistent with $Q_{\rm Z'}$ being a local approximation of the Q-factor around the tuned resonance frequency and hence it is more accurate for relatively narrow fractional bandwidths $B \ll 1/Q$ or equivalently $\Gamma_0 \ll 1$. The Q factors from $Q_{\rm C}$

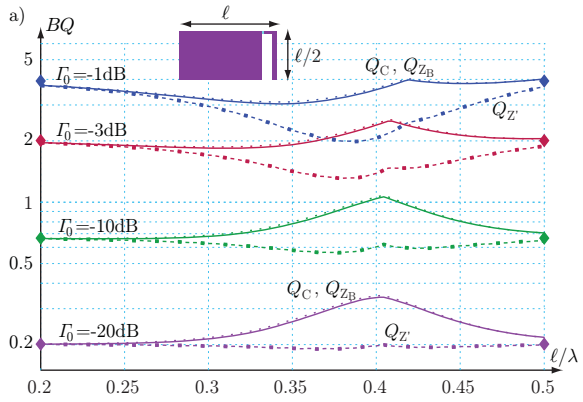

Fig. 9. Illustration of the Q-factor fractional bandwidth product for the inverted L antenna using the Q-factor from the current expressions $Q_{\rm C}$, energy in the Brune synthesized lumped circuit model $Q_{\rm Z_B}$, and differentiation of the input impedance $Q_{\rm Z'}$. The bandwidth is determined for the thresholds $\Gamma_0 = -\{1, 3, 10, 20\}$ dB corresponding to the fractional bandwidths $B \approx \{48, 32, 14, 4.6\}$% at $\ell/\lambda = 0.4$.

and $Q_{\rm Z_B}$ underestimate the fractional bandwidths for this case. The accuracy of $Q_{\rm Z'}$ deteriorates as the threshold Γ_0 is relaxed due to the difficulties to approximate the input impedance with a resonance circuit over large bandwidths. The results for the Q-factor determined from the stored energy $Q_{\rm C} \approx Q_{\rm Z_B}$ are on the contrary improving as the requirements on the matching are relaxed. This is consistent with $Q_{\rm Z_B}$ being a global quantity determined from the input impedance over a large bandwidth.

Matching networks can be used to increase the bandwidth B for a given matching threshold Γ_0 or to decrease the matching threshold Γ_0 for a fixed bandwidth B. The Bode-Fano limits [24] are useful for simple circuits such as the RCL resonance circuit. The increasing complexity of the Bode-Fano limits prohibits its use for general circuits. Here, we instead consider the real frequency technique to determine the optimal parameter values [40]. The resulting reflection coefficient is approximately -12 dB and -6 dB for the $B = 2/\langle Q \rangle$ and $B = 4/\langle Q \rangle$ cases, respectively, where $\langle Q \rangle$ denotes the mean $\langle Q \rangle = (Q_{\rm C} + Q_{\rm Z'})/2$. It is noted that $Q_{\rm C}$ and $Q_{\rm Z'}$ are most accurate for the wide and narrow bandwidths, respectively.

V. Conclusions

The energy expressions proposed by Vandenbosch in [7] are very well suited for optimization formulations as they are simple quadratic forms of the current density. The quadratic form is very practical as it allows for various optimization formulations such as Lagrangian [9] and convex optimization [11] and has already led to many new antenna results. Their resemblance of the electric field integral equation (EFIE) makes the numerical implementation very simple.

Numerical results for dipole, bow-tie, loop, and inverted L antennas are used to illustrate the accuracy of the energy expressions. The Q-factors from the stored energy in the fields, $Q_{\rm C}$, from the stored energy in Brune synthesized circuit models, $Q_{\rm Z_B}$, and from differentiation of the input impedance, $Q_{\rm Z'}$ are compared. It is observed that $Q_{\rm C} \approx Q_{\rm Z_B}$ for the

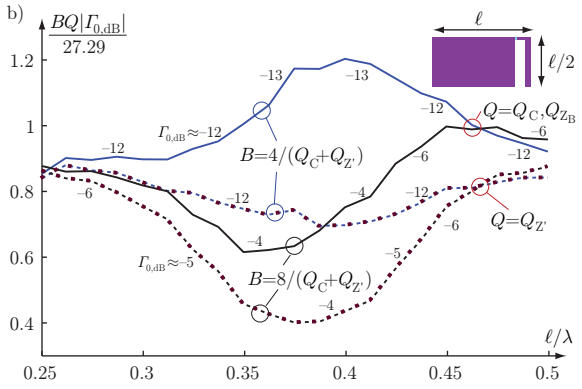

Fig. 10. Illustration of the Q-factor fractional bandwidth product for the inverted L antenna using the Q factors from the far-field stored energy Q_{C}, energy in the Brune synthesized lumped circuit model $Q_{\mathrm{Z_B}}$, and differentiation of the input impedance $Q_{\mathrm{Z}'}$. The matching threshold Γ_0 is determined using the real frequency technique [40] over the fractional bandwidths $B=\{2,4\}/\langle Q\rangle$, where $\langle Q\rangle$ is the mean $\langle Q\rangle=(Q_{\mathrm{C}}+Q_{\mathrm{Z}'})/2$. The resulting Γ_0 are approximately $\Gamma_0\approx -12\,\mathrm{dB}$ for $B=2/\langle Q\rangle$ and $-6\,\mathrm{dB}$ to $-4\,\mathrm{dB}$ for $B=2/\langle Q\rangle$ as indicated in the graph.

considered cases. The good agreement is based on Brune circuits synthesized from the input impedance over a wide frequency range and it is observed that $Q_{\mathrm{Z_B}}$ can be lower if a narrow range of frequencies is used. We also observe that $Q_{\mathrm{C}}\approx Q_{\mathrm{Z_B}}\approx Q_{\mathrm{Z}'}$ in the regions where the Q-factor is $Q_{\mathrm{C}}\geq 10$ and that $Q_{\mathrm{Z}'}\leq Q_{\mathrm{C}}\approx Q_{\mathrm{Z_B}}$ otherwise. This is consistent with the shunt and series resonance circuit that can have $Q_{\mathrm{Z}'}=0$ although $Q_{\mathrm{Z_B}}\gg 1$, see (17) and [22]. The numerical results also show that the modification of the stored energy in [41] by addition of ka increases the deviation from $Q_{\mathrm{Z_B}}$. For example, the Q_{C} for the strip dipole in Fig. 5 and bow-tie in Fig. 6 would increase with approximately $ka=2\pi\approx 6.3$ for $\ell/\lambda=2$.

Appendix A
Brune Synthesis

One problem with the Brune synthesis is that it uses negative inductors and capacitors [21, 36], see also Fig. 2. This is resolved by transforming the *Tee* network containing the negative element to an ideal transformer, see Fig. 11, where $L_1<0$. The inductors in the ideal transformer are $M=L_3$, $L_{\mathrm{a}}=L_1+L_3$, and $L_{\mathrm{b}}=L_2+L_3\geq 0$. From the Brune synthesis [21, 36], it follows that the inductors are related as $L_1L_2+L_1L_3+L_2L_3=0$, and hence $L_{\mathrm{a}}L_{\mathrm{b}}=L_3^2$ showing that $L_{\mathrm{a}}>0$. The stored magnetic energy in the *Tee* network and ideal transformer in Fig. 11 is

$$W^{(\mathrm{M})}=\frac{|I_1|^2L_1}{4}+\frac{|I_2|^2L_2}{4}+\frac{|I_1+I_2|^2L_3}{4}=\frac{|I_1|^2L_{\mathrm{a}}}{4}+\frac{|I_2|^2L_{\mathrm{b}}}{4}+\frac{\mathrm{Re}\{I_1I_2^*\}M}{2}. \quad (18)$$

The corresponding stored electric energy is $W^{(\mathrm{E})}=|I_1+I_2|^2/(4\omega^2C)$ showing that the stored energy in the ideal transformer is identical to the stored energy in the original circuit representation.

The interpretation for the case $X_{\mathrm{B}}>0$ is more involved [21, 36]. Here, the Π network with a negative capacitance C_1 and positive capacitances C_2, C_3 are first transformed to a *Tee* network with the components $C=C_1+C_2$, $L_1=LC_2/C$, $L_2=LC_1/C$, $L_3=LC_3/C$, see Fig. 12. The stored energies are not the same in the Π and *Tee* networks for general component values. However, the components are not arbitrary in the Brune synthesis [21, 36]. The capacitors in the Π network are constrained as $C_1C_2+C_1C_3+C_2C_3=0$ and the inductors in the *Tee* network satisfy $L_1L_2+L_1L_3+L_2L_3=0$. The stored energies are identical for this case. The *Tee* network is finally transformed to an ideal transformer, see Fig. 11. We consider the stored electric energy to see that the stored energies are identical for the Brune case. With prescribed voltages V_1 and V_2, we have

$$\begin{aligned}4W^{(\mathrm{E})}&=|V_1|^2C_1+|V_2|^2C_2+|V_1-V_2|^2C_3\\&=|V_1|^2C_1+|V_2|^2C_2-|V_1-V_2|^2\frac{C_1C_2}{C_1+C_2}\\&=\frac{|C_1V_1+C_2V_2|^2}{C_1+C_2}=\frac{|C_1V_1+C_2V_2|^2}{C}\end{aligned} \quad (19)$$

for the Π network, where $C_1C_2+C_1C_3+C_2C_3=0$ is used. The stored energy in the corresponding *Tee* network is

$$4W^{(\mathrm{E})}=\frac{|V|^2}{|\omega L_3-\frac{1}{\omega C}|^2\omega^2C}=\frac{|V|^2C}{|\omega^2LC_3-1|^2} \quad (20)$$

where V is the voltage

$$\begin{aligned}V&=\frac{\frac{V_1}{\mathrm{j}\omega L_1}+\frac{V_2}{\mathrm{j}\omega L_2}}{\frac{1}{\mathrm{j}\omega L_1}+\frac{1}{\mathrm{j}\omega L_2}+\frac{1}{\mathrm{j}\omega L_3+\frac{1}{\mathrm{j}\omega C}}}=\frac{C_1V_1+C_2V_2}{C+\frac{C_1C_2}{C_3-\frac{1}{\omega^2L}}}\\&=(C_1V_1+C_2V_2)\frac{\omega^2LC_3-1}{C}\end{aligned} \quad (21)$$

that inserted into (20) gives (19) and shows that the stored electric energies are identical for the Π and *Tee* networks for the case $C_1C_2+C_1C_3+C_2C_3=0$. The *Tee* network has a negative inductance L_2 that is removed in the final transformation to the ideal transformer, see Fig. 11.

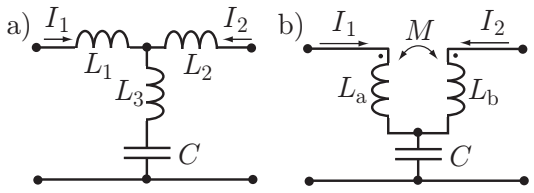

Fig. 11. Transformation of the *Tee* network (a) to an ideal transformer (b).

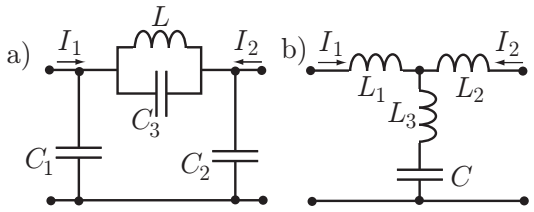

Fig. 12. Transformation of the Π network (a) to a *Tee* network (b).

APPENDIX B
BODE-FANO MATCHING LIMITATIONS

We consider the Bode-Fano matching limitations [22, 24–26] for the cascaded shunt LC and series LC circuit in Fig. 3. Using the asymptotic expansions and the zeros in the complex half plane, we have the integral identities

$$\frac{2}{\pi}\int_0^\infty \omega^2 \ln\frac{1}{|\Gamma(\omega)|}\,\mathrm{d}\omega = \frac{2}{Q_\mathrm{e}} + \frac{2}{3}\sum_n \lambda_n^3 \tag{22}$$

$$\frac{2}{\pi}\int_0^\infty \ln\frac{1}{|\Gamma(\omega)|}\,\mathrm{d}\omega = \frac{2}{Q_\mathrm{g}} - 2\sum_n \lambda_n \tag{23}$$

$$\frac{2}{\pi}\int_0^\infty \frac{1}{\omega^2}\ln\frac{1}{|\Gamma(\omega)|}\,\mathrm{d}\omega = \frac{2}{Q_\mathrm{g}} - 2\sum_n \frac{1}{\lambda_n} \tag{24}$$

$$\frac{2}{\pi}\int_0^\infty \frac{1}{\omega^4}\ln\frac{1}{|\Gamma(\omega)|}\,\mathrm{d}\omega = \frac{2}{Q_\mathrm{e}} + \frac{2}{3}\sum_n \frac{1}{\lambda_n^3} \tag{25}$$

where $Q_\mathrm{g} = \max\{Q_\mathrm{p}, Q_\mathrm{s}\}$, $Q_\mathrm{l} = \min\{Q_\mathrm{p}, Q_\mathrm{s}\}$, $Q_\mathrm{e} = 3Q_\mathrm{g}^3Q_\mathrm{l}/(3Q_\mathrm{g}^2Q_\mathrm{l} + 3Q_\mathrm{g} - Q_\mathrm{l}) \le Q_\mathrm{g}$, $\mathrm{Re}\,\lambda_n \ge 0$, and we have assumed that $\omega_0 = 1$. We bound the integrals using $\max_\omega |\Gamma(\omega)| = \Gamma_0$ for $\omega \in \omega_0[1 - B/2, 1 + B/2]$ giving the inequalities

$$\frac{1}{\pi}(B + B^3/12)\ln\frac{1}{|\Gamma_0|} \le \frac{1}{Q_\mathrm{e}} + \frac{1}{3}\sum_n \lambda_n^3 \tag{26}$$

$$\frac{1}{\pi}B\ln\frac{1}{|\Gamma_0|} \le \frac{1}{Q_\mathrm{g}} - \sum_n \lambda_n \tag{27}$$

$$\frac{1}{\pi}\frac{B}{1 - B^2/4}\ln\frac{1}{|\Gamma_0|} \le \frac{1}{Q_\mathrm{g}} - \sum_n \frac{1}{\lambda_n} \tag{28}$$

$$\frac{1}{\pi}\frac{B + B^3/12}{(1 - B^2/4)^3}\ln\frac{1}{|\Gamma_0|} \le \frac{1}{Q_\mathrm{e}} + \frac{1}{3}\sum_n \frac{1}{\lambda_n^3} \tag{29}$$

We note that the middle equations are identical to the Bode-Fano bound for the RCL circuit [22] for maximal Q value $\max\{Q_\mathrm{p}, Q_\mathrm{s}\}$. This is natural as the cascaded shunt (or series) circuit cannot improve the matching. It is also seen that a complex conjugate pair gives the optimal λ_n for $B \ll 1$ and that this case reduces to the bound for the RCL circuit. The set of inequalities are solved numerically for Γ_0 given B and assuming a complex conjugate pair λ_n, see Fig. 3.

REFERENCES

[1] L. J. Chu, "Physical limitations of omnidirectional antennas," *J. Appl. Phys.*, vol. 19, pp. 1163–1175, 1948.

[2] R. E. Collin and S. Rothschild, "Evaluation of antenna Q," *IEEE Trans. Antennas Propagat.*, vol. 12, pp. 23–27, Jan. 1964.

[3] H. D. Foltz and J. S. McLean, "Limits on the radiation Q of electrically small antennas restricted to oblong bounding regions," in *IEEE Antennas and Propagation Society International Symposium*, vol. 4. IEEE, 1999, pp. 2702–2705.

[4] J. C.-E. Sten, P. K. Koivisto, and A. Hujanen, "Limitations for the radiation Q of a small antenna enclosed in a spheroidal volume: axial polarisation," *AEÜ Int. J. Electron. Commun.*, vol. 55, no. 3, pp. 198–204, 2001.

[5] H. L. Thal, "New radiation Q limits for spherical wire antennas," *IEEE Trans. Antennas Propagat.*, vol. 54, no. 10, pp. 2757–2763, Oct. 2006.

[6] A. D. Yaghjian and S. R. Best, "Impedance, bandwidth, and Q of antennas," *IEEE Trans. Antennas Propagat.*, vol. 53, no. 4, pp. 1298–1324, 2005.

[7] G. A. E. Vandenbosch, "Reactive energies, impedance, and Q factor of radiating structures," *IEEE Trans. Antennas Propagat.*, vol. 58, no. 4, pp. 1112–1127, 2010.

[8] ——, "Simple procedure to derive lower bounds for radiation Q of electrically small devices of arbitrary topology," *IEEE Trans. Antennas Propagat.*, vol. 59, no. 6, pp. 2217–2225, 2011.

[9] M. Gustafsson, M. Cismasu, and B. L. G. Jonsson, "Physical bounds and optimal currents on antennas," *IEEE Trans. Antennas Propagat.*, vol. 60, no. 6, pp. 2672–2681, 2012.

[10] M. Capek, P. Hazdra, and J. Eichler, "A method for the evaluation of radiation Q based on modal approach," *IEEE Trans. Antennas Propagat.*, vol. 60, no. 10, pp. 4556–4567, 2012.

[11] M. Gustafsson and S. Nordebo, "Optimal antenna currents for Q, superdirectivity, and radiation patterns using convex optimization," *IEEE Trans. Antennas Propagat.*, vol. 61, no. 3, pp. 1109–1118, 2013.

[12] M. Cismasu and M. Gustafsson, "Antenna bandwidth optimization with single frequency simulation," *IEEE Trans. Antennas Propagat.*, vol. 62, no. 3, pp. 1304–1311, 2014.

[13] ——, "Multiband antenna Q optimization using stored energy expressions," *IEEE Antennas and Wireless Propagation Letters*, vol. 13, no. 2014, pp. 646–649, 2014.

[14] P. Hazdra, M. Capek, and J. Eichler, "Radiation Q-factors of thin-wire dipole arrangements," *Antennas and Wireless Propagation Letters, IEEE*, vol. 10, pp. 556–560, 2011.

[15] S. M. Mikki and Y. M. Antar, "A theory of antenna electromagnetic near field part I," *IEEE Trans. Antennas Propagat.*, vol. 59, no. 12, pp. 4691–4705, 2011.

[16] M. Gustafsson and B. L. G. Jonsson, "Stored electromagnetic energy and antenna Q," Lund University, Department of Electrical and Information Technology, P.O. Box 118, S-221 00 Lund, Sweden, Tech. Rep. LUTEDX/(TEAT-7222)/1–25/(2012), 2012, http://www.eit.lth.se.

[17] W. Geyi, "On stored energies and radiation Q," *arXiv preprint arXiv:1403.3129*, 2014.

[18] A. D. Yaghjian, M. Gustafsson, and B. L. G. Jonsson, "Minimum Q for lossy and lossless electrically small dipole antennas," *Progress In Electromagnetics Research*, vol. 143, pp. 641–673, 2013.

[19] M. Gustafsson, D. Tayli, and M. Cismasu, "Q factors for antennas in dispersive media," Lund University, Department of Electrical and Information Technology, P.O. Box 118, S-221 00 Lund, Sweden, Tech. Rep. LUTEDX/(TEAT-7232)/1–24/(2014), 2014, http://www.eit.lth.se.

[20] B. L. G. Jonsson and M. Gustafsson, "Stored energies in electric and magnetic current densities for small antennas," arXiv:1410.8704 (2014).

[21] O. Wing, *Classical Circuit Theory*. New York: Springer, 2008.

[22] M. Gustafsson and S. Nordebo, "Bandwidth, Q factor, and resonance models of antennas," *Progress in Electromagnetics Research*, vol. 62, pp. 1–20, 2006.

[23] H. Stuart, S. Best, and A. Yaghjian, "Limitations in relating quality factor to bandwidth in a double resonance small antenna," *Antennas and Wireless Propagation Letters*, vol. 6, 2007.

[24] R. M. Fano, "Theoretical limitations on the broadband matching of arbitrary impedances," *Journal of the Franklin Institute*, vol. 249, no. 1,2, pp. 57–83 and 139–154, 1950.

[25] M. C. Villalobos, H. D. Foltz, and J. S. McLean, "Broadband matching limitations for higher order spherical modes," *IEEE Trans. Antennas Propagat.*, vol. 57, no. 4, pp. 1018–1026, 2009.

[26] B. Kogan, "Comments on "Broadband matching limitations for higher order spherical modes"," *IEEE Trans. Antennas Propagat.*, vol. 58, no. 5, p. 1826, 2010.

[27] M. Capek, L. Jelinek, P. Hazdra, and J. Eichler, "The Measurable Q Factor and Observable Energies of Radiating Structures," *IEEE Trans. Antennas Propagat.*, vol. 62, no. 1, pp. 311–318, Jan 2014.

[28] R. L. Fante, "Quality factor of general antennas," *IEEE Trans. Antennas Propagat.*, vol. 17, no. 2, pp. 151–155, Mar. 1969.

[29] R. Harrington, "Characteristic modes for antennas and scatterers," in *Numerical and Asymptotic Techniques in Electromagnetics*, ser. Topics in Applied Physics, R. Mittra, Ed. Springer Berlin Heidelberg, 1975, vol. 3, pp. 51–87.

[30] W. Geyi, "Optimization of the ratio of gain to Q," *IEEE Trans. Antennas Propagat.*, vol. 61, no. 4, pp. 1916–1922, 2013.

[31] H. L. Thal, "Q Bounds for Arbitrary Small Antennas: A Circuit Approach," *IEEE Trans. Antennas Propagat.*, vol. 60, no. 7, pp. 3120–3128, 2012.

[32] W. Geyi, "A method for the evaluation of small antenna Q," *IEEE Trans. Antennas Propagat.*, vol. 51, no. 8, pp. 2124–2129, 2003.

[33] J. S. McLean, "A re-examination of the fundamental limits on the radiation Q of electrically small antennas," *IEEE Trans. Antennas Propagat.*, vol. 44, no. 5, pp. 672–676, May 1996.

[34] A. D. Yaghjian, "Internal energy, Q-energy, Poynting's theorem, and the stress dyadic in dispersive material," *IEEE Trans. Antennas Propagat.*, vol. 55, no. 6, pp. 1495–1505, 2007.
[35] W. Geyi, *Foundations of Applied Electrodynamics*. John Wiley & Sons, 2011.
[36] O. Brune, "Synthesis of a finite two-terminal network whose driving-point impedance is a prescribed function of frequency," *MIT J. Math. Phys.*, vol. 10, pp. 191–236, 1931.
[37] B. Gustavsen and A. Semlyen, "Rational approximation of frequency domain responses by vector fitting," *Power Delivery, IEEE Transactions on*, vol. 14, no. 3, pp. 1052–1061, 1999.
[38] B. Gustavsen, "Fast passivity enforcement for s-parameter models by perturbation of residue matrix eigenvalues," *Advanced Packaging, IEEE Transactions on*, vol. 33, no. 1, pp. 257–265, 2010.
[39] Y. Rahmat-Samii and E. Michielssen, *Electromagnetic Optimization by Genetic Algorithms*, ser. Wiley Series in Microwave and Optical Engineering. John Wiley & Sons, 1999.
[40] H. J. Carlin and P. P. Civalleri, *Wideband circuit design*. Boca Raton: CRC Press, 1998.
[41] G. A. E. Vandenbosch, "Radiators in time domain, part II: finite pulses, sinusoidal regime and Q factor," *IEEE Trans. Antennas Propagat.*, vol. 61, no. 8, pp. 4004–4012, 2013.

Mats Gustafsson (M'05) received the M.Sc. degree in Engineering Physics 1994, the Ph.D. degree in Electromagnetic Theory 2000, was appointed Docent 2005, and Professor of Electromagnetic Theory 2011, all from Lund University, Sweden.

He co-founded the company Phase holographic imaging AB in 2004. His research interests are in scattering and antenna theory and inverse scattering and imaging with applications in microwave tomography and digital holography. He has written over 75 peer reviewed journal papers and over 90 conference papers. Prof. Gustafsson received the Best Antenna Poster Prize at EuCAP 2007, the IEEE Schelkunoff Transactions Prize Paper Award 2010, and the Best Antenna Theory Paper Award at EuCAP 2013. He serves as an IEEE AP-S Distinguished Lecturer for 2013-15.

Lars Jonsson received the M.Sc. degree in Engineering Physics from Ume University, Sweden, in 1995, and the Ph.D. degree in Electromagnetic Theory in 2001 from Royal Institute of Technology (KTH), Stockholm, Sweden. He was a postdoctoral fellow at University of Toronto, Canada and a Wissenschaftlicher Mitarbeiter (postdoc) at ETH Zurich, Switzerland. Since 2006, he has been with the Electromagnetic Engineering Lab at Royal Institute of Technology (KTH) where he was an Assistant Professor and was appointed Docent in Electromagnetic Theory and he became Associate Professor both in Nov 2006. His research interests include electromagnetic theory in a wide sense, including scattering, antenna theory and nonlinear dynamics.